Taylor & Francis
Taylor & Francis Group

Non-linear Oscillations of Milling

B. BALACHANDRAN* and D. GILSINN

National Institute of Standards and Technology, Gaithersburg, MD, USA.

The principal features of two mathematical models that can be used to study non-linear oscillations of a workpiece–tool system during a milling operation are presented and explained in this article. These models are non-linear, non-homogeneous, delay-differential systems with time-periodic coefficients. In the treatment presented here, the sources of non-linearities are the multiple regenerative effect and the loss-of-contact effect. The time-delay effect is taken into account, and the dependence of this delay effect on the feed rate is modelled. A variable time delay is introduced to capture the influence of the feed-rate in one of the models. Two formulations that can be used to carry out stability analysis of periodic solutions are presented. The models presented and the stability-analysis formulations are relevant for predicting and understanding chatter in milling.

Keywords: Milling, chatter, variable time delay, loss of contact.

1 Introduction

For more than a decade, there has been a push towards using high-speed machining technology in aerospace, automobile, electronics, and other industries [1]–[3]. High-speed milling (HSM), a high-speed machining technology, can be loosely used to cover milling operations where the parameter values satisfy one or more of the following: (a) spindle speeds of 2094.4 rad/s [20,000 revolutions per minute (rpm)] and higher rpm, (b) cutting speeds of 50 m/s and higher speeds, and (c) feed rates of 1 m/s and higher rates. (These parameter values are to be considered as representative standards, since the cutting speeds for HSM vary from one workpiece material to another and the spindle rpm for HSM vary with spindle taper size.) High-speed milling has the benefit of increased metal removal rate and many other benefits (e.g. see [4]). Due to many attractive aspects, high-speed milling is increasingly viewed as a viable alternative to other forms of manufacturing. For example, in several industries, such as the aerospace industry, HSM capabilities allow for design concepts such as unitized assemblies,

*Corresponding author. B. Balachandran, Department of Mechanical Engineering, University of Maryland, College Park, MD 20742, USA.

thinner structural elements for weight reduction, and substantially reduced require-
ments for deburring and hand-finishing machined components.

The models presented here are aimed at obtaining a better understanding of the
system dynamics during a high-speed milling operation. During a milling process,
chatter is an undesired relative oscillation between the workpiece and the tool that can
result in poor accuracy and tool wear and also limit the material removal rate. Hence,
considerable attention has been devoted to understanding chatter mechanisms,
predicting the onset of chatter, and suppressing chatter. As in self-excited systems,
there is a regenerative effect in a milling process. This effect is in the form of a time-
delay effect in the governing equations, and the physical source of this effect is the
cutting force in the workpiece – tool system. This force depends on the chip thickness,
which is determined not only by the present state of motion of the workpiece – tool
system but also by the past state of motion of this system. In the context of milling
processes, considerable research on chatter due to this time-delay effect has been
carried out ([5] – [14]).

In general, the governing system of equations of a milling process is a non-linear,
non-homogeneous, delay-differential system with time-periodic coefficients [12, 13, 14].
Over the years, this system of equations has been approximated on a physical basis as
well as a mathematical basis to determine the stability of motions of the workpiece –
tool system. These approximations deal with consideration of non-linearities, the time-
periodic nature of the cutting-force coefficients, and the feed terms. For example, if one
does not consider multiple regenerative effects, loss-of-contact dynamics, friction,
structural non-linearities, and other sources of non-linearities, then the resulting system
of equations is linear [5, 7, 8, 10, 11]. In the work of Hanna and Tobias [9], face milling
processes were considered and it was modelled with structural non-linearities and
cutting-force non-linearities. Quadratic and cubic non-linearities were included in a
delay-differential system with constant coefficients, and the stability of the zero
solution of this system was studied. Hahn [15] presented an extension of Floquet's
theorem for delay-differential equations with periodic coefficients. This provided a
basis for the work of Sridhar et al. [8] who numerically computed the fundamental
matrix and the eigenvalues of this matrix. In the study of Minis and Yanushevsky [10],
as in previous studies [8, 11], milling operations with straight fluted cutters are
considered. They used Floquet theory to determine the stability of the zero solution of
a linear, homogeneous delay-differential system. The periodic terms were expanded by
using a Fourier expansion with the basic frequency defined by the spindle speed. The
Hill determinant (Nayfeh and Mook [16]) was obtained, and zeroth-order and first-
order truncations of the resulting characteristic equation were used in determining the
stability charts in the space of spindle speed and depth of cut.

While linear models are useful for predicting the onset of chatter, they are not suited
for understanding the nature of the instability and post-instability motions. In the
work of Balachandran and Zhao [13] and Zhao and Balachandran [14], loss-of-contact
non-linearities and feed rate effects are considered. They pointed out that linear models
can provide quite accurate stability predictions for high-immersion milling operations,
but inaccurate stability predictions for low-immersion operations. Stability of these
operations in the space of spindle speed and depth of cut can be constructed through
time-domain simulations of this non-linear system. However, for determining the type
of instability of the periodic motion of this non-linear, non-homogeneous, non-
autonomous, delay-differential system, numerical schemes with an analytical basis are
required. One example of this scheme is the semi-discretization scheme as presented
recently [17, 18]. This scheme has been shown to be an efficient numerical scheme for

studying the stability of the zero solution of non-autonomous systems with a continuous time delay. An alternate formulation that can be used to determine the stability of a periodic orbit of a delay-differential system is based on the integral operator approach [19].

Given the tutorial nature of this article, we have not tried to provide a comprehensive list of all of the references related to milling dynamics. Primary contributions of this article include the following: (a) presentation of a variable time-delay model for a milling process, and (b) a semi-discretization treatment and an integral operator formulation that can be used for stability analysis of systems with multiple delays. In section 2, two models are presented, and in section 3, two stability-analysis formulations are explored. Representative stability chart results are presented in section 4. Finally, concluding remarks are presented.

2 MODELS OF MILLING PROCESSES

A multi-degree-of-freedom model of a workpiece – tool system is illustrated in figure 1. The feed direction and spindle rotation are shown for a down-milling operation with a cylindrical end mill. (For the same feed direction, if the spindle rotation is reversed, the operation is called an up-milling operation.) The tool and the workpiece are each represented by an equivalent two-degree-of-freedom spring – mass – damper system, and the respective motions are described by coordinates as shown in the figure. The cutting tool has a radius of R, N number of flutes, and a helix angle η. (The helix angle
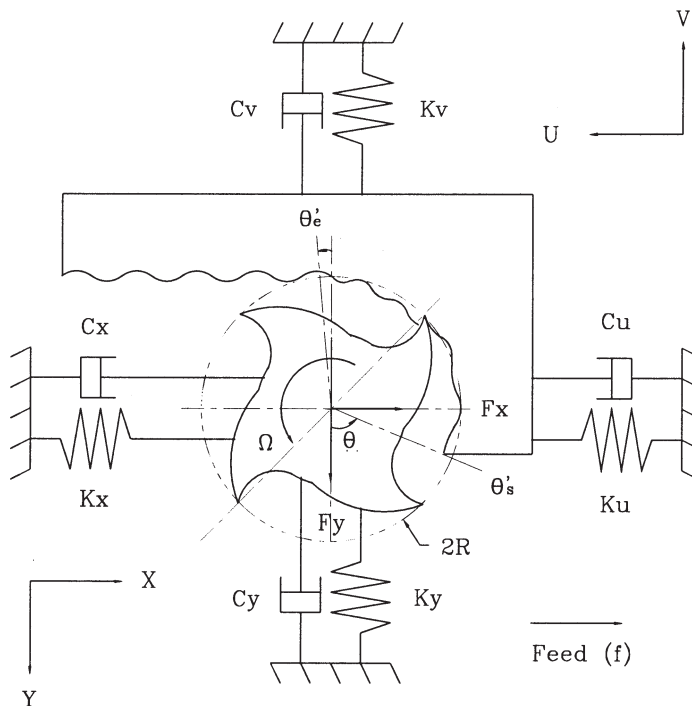
Figure 1. Workpiece – tool system model.

Figure 2. End mill and a disk element.

is shown in figure 2.) For convenience, it is assumed that the cutter translates along the X direction with a feed rate f. The vertical axis of the tool is oriented along the Z direction. Forces F_x and F_y act on the cutter, and forces F_u and F_v act on the workpiece. The spindle rotational speed is represented by Ω.

Here, the primary interest is in the dynamics on the horizontal plane. Furthermore, the resonance frequencies associated with the torsion modes and the Z-direction vibration modes are expected to be higher than those associated with the other modes. For these reasons, only the vibration modes in the horizontal plane are considered in the models presented in sections 2.1 and 2.2. In developing these models, it is assumed that the modal properties of the tool and the workpiece are obtained from experimental modal analysis and/or finite-element analyses. Thus a system with a flexible tool and a flexible workpiece is represented by an equivalent lumped parameter system.

2.1   Model with Two Time Delays

For the system shown in figure 1, the differential equations governing the motions of the workpiece–tool system can be written in the form [12, 13]

$$
\begin{aligned}
m_x \ddot{q}_x &+ c_x \dot{q}_x &+ k_x q_x &= F_x(t; \tau_1, \tau_2) \\
m_y \ddot{q}_y &+ c_y \dot{q}_y &+ k_y q_y &= F_y(t; \tau_1, \tau_2) \\
m_u \ddot{q}_u &+ c_u \dot{q}_u &+ k_u q_u &= F_u(t; \tau_1, \tau_2) \\
m_v \ddot{q}_v &+ c_v \dot{q}_v &+ k_v q_v &= F_v(t; \tau_1, \tau_2)
\end{aligned}
\tag{1}
$$

where the tool degrees of freedom q_x and q_y are the displacements in an inertial reference frame along the X and Y directions, respectively; the workpiece degrees of

freedom q_u and q_v are the displacements in an inertial reference frame along the U and V directions, respectively; and t denotes time. The cutting force components, which appear on the right-hand side of the equations, are time-periodic functions. The discrete time delays τ_1 and τ_2, which are introduced in the governing equations through the cutting force components, are minimal tool-pass periods along the X and Y directions, respectively. As discussed later in this section, these delays depend on the feed rate and the spindle rotation speed. (It needs to be recognized that the introduction of the two explicitly defined delays is an approximation of the actual situation where one numerically determined delay may suffice to determine when a tool returns to the same engagement position with the workpiece.) The dependences of the cutting force components on the system states are not explicitly shown in equations (1).

Although the form of equations (1) is sufficient for studying the dynamics and stability of a milling operation, to determine the displacement fields associated with the tool and the workpiece, one will need information about the corresponding mode shapes. It has been assumed that the respective principal directions associated with the tool vibration modes and the workpiece vibration modes are parallel to each other. This aspect may not be necessarily true of all milling systems. However, the displacements associated with the respective vibration modes can always be decomposed in terms of the degrees of freedom along the X, Y, U, and V directions shown in figure 1. It also needs to be noted that here, the feed direction has been assumed to be parallel to a direction associated with an essential degree of freedom of the tool (or the workpiece). This feature is also not representative of all milling operations.

In the cutting zone $\theta_s\prime < \theta(i,t,z) < \theta_e\prime$ (see figure 1), when the ith cutting tooth is in contact with workpiece, the corresponding cutting force components are given by

$$\left\{ \begin{array}{c} F_x^i(t;\tau_1,\tau_2) \\ F_y^i(t;\tau_1,\tau_2) \end{array} \right\} = \begin{bmatrix} \kappa_{11}^i(t) & \kappa_{12}^i(t) \\ \kappa_{21}^i(t) & \kappa_{22}^i(t) \end{bmatrix} \left\{ \begin{array}{c} A(t;\tau_1) \\ B(t;\tau_2) \end{array} \right\} + \begin{bmatrix} c_{11}^i(t) & c_{12}^i(t) \\ c_{21}^i(t) & c_{22}^i(t) \end{bmatrix} \left\{ \begin{array}{c} \dot{A}(t;\tau_1) \\ \dot{B}(t;\tau_2) \end{array} \right\} \quad (2)$$

where the relative displacement functions are given by

$$\begin{aligned} A(t;\tau_1) &= q_x(t) - q_x(t - l\tau_1) + q_u(t) - q_u(t - l\tau_1) + lf\tau_1 \\ B(t;\tau_2) &= q_y(t) - q_y(t - l\tau_2) + q_v(t) - q_v(t - l\tau_2) \end{aligned} \quad (3)$$

In equations (2), both stiffness terms and damping terms are taken into account. In equations (3), l is a positive integer that is associated with what is called the multiple regenerative effect.

When a cutting flute is outside the cutting zone, then the cutting force components associated with this flute are zero. In addition, when the dynamic uncut chip thickness associated with the ith flute is zero, then there is no contact between the workpiece and the corresponding cutter flute. The corresponding cutting force components are zero when there is loss of contact; that is,

$$\left\{ \begin{array}{c} F_x^i(t;\tau_1,\tau_2) \\ F_y^i(t;\tau_1,\tau_2) \end{array} \right\} = \mathbf{0} \quad (4)$$

This loss of contact is one source of non-linearity.

Carrying out a summation over the N cutting flutes, the cutting force is determined to be

$$\begin{Bmatrix} F_x(t;\tau_1,\tau_2) \\ F_y(t;\tau_1,\tau_2) \end{Bmatrix} = \sum_{i=1}^{N} \begin{Bmatrix} F_x^i(t;\tau_1,\tau_2) \\ F_y^i(t;\tau_1,\tau_2) \end{Bmatrix}$$

$$= \begin{bmatrix} \kappa_{11}(t) & \kappa_{12}(t) \\ \kappa_{21}(t) & \kappa_{22}(t) \end{bmatrix} \begin{Bmatrix} A(t;\tau_1) \\ B(t;\tau_2) \end{Bmatrix} \tag{5}$$

$$+ \begin{bmatrix} c_{11}(t) & c_{12}(t) \\ c_{21}(t) & c_{22}(t) \end{bmatrix} \begin{Bmatrix} \dot{A}(t;\tau_1) \\ \dot{B}(t;\tau_2) \end{Bmatrix}$$

In addition, from Newton's third law of motion, the forces acting on the workpiece can be determined as

$$\begin{Bmatrix} F_u(t;\tau_1,\tau_2) \\ F_v(t;\tau_1,\tau_2) \end{Bmatrix} = \begin{Bmatrix} F_x(t;\tau_1,\tau_2) \\ F_y(t;\tau_1,\tau_2) \end{Bmatrix} \tag{6}$$

When the feed rate is significant, the tool-pass period is likely to be different along the X and Y directions of figure 1. Let the tool-pass period along the X direction be

$$\tau_1 = T = \frac{1}{N\Omega} \tag{7}$$

where Ω is the spindle speed. Then, based on quasi-static approximations, the tool-pass period along the Y direction can be determined as

$$\tau_2 = \frac{4\pi R}{N(4\pi\Omega R + f)} \tag{8}$$

The difference between τ_1 and τ_2 is due to the feed along one of the directions. The model with two explicitly defined time delays can be considered as an approximation of the variable time delay model presented in section 2.2.

The cutter is modelled as a stack of infinitesimal disk elements, and in figure 2 one of these elements, which is located at an axial distance z along the tool where $0 < z <$ axial depth of cut (ADOC), is shown. The cutting force components associated with this disk element are represented by ΔF_r for the radial direction, ΔF_t for the tangential direction, and ΔF_z for the axial direction. To determine the cutting force component along the radial direction, the dynamic uncut chip thickness for the ith flute of the cutter at time t and height z is determined from

$$h(t,i,z;\tau_1,\tau_2) = A(t;\tau_1)\sin\theta(t,i,z) + B(t;\tau_2)\cos\theta(t,i,z) \tag{9}$$

where the relative displacements are given by equations (3), the variable $\theta(t, i, z)$, which is the angular position of tooth i at axial location z and time t, is given by

$$\theta(t,i,z) = 2\pi\Omega t - (i-1)\frac{2\pi}{N} - \frac{\tan\eta}{R}z + \theta_0 \tag{10}$$

where θ_0 is the initial angular position of the first tooth at $z = 0$.

In equation (3), the positive integer l is the number of a previous tooth pass period associated with maximum relative radial displacement between the tool and the

workpiece as they move towards each other. In the simulations, the value of l is determined from the following relations in which a limited number of the delay terms have been included.

$$
\begin{aligned}
q_x(t - l\tau_1) - lf\tau_1 + q_u(t - l\tau_1) &= \max\{q_x(t - \tau_1) - f\tau_1 + q_u(t - \tau_1), \\
&\qquad q_x(t - 2\tau_1) - 2f\tau_1 + q_u(t - 2\tau_1), \ldots\} \\
q_y(t - l\tau_2) + q_v(t - l\tau_2) &= \max\{q_y(t - \tau_2) + q_v(t - \tau_2), \\
&\qquad q_y(t - 2\tau_2) + q_v(t - 2\tau_2), \ldots\}
\end{aligned}
\tag{11}
$$

Equations (11) capture a non-linearity associated with what is called the multiple regenerative effect. While this effect can be studied through numerical simulations, this effect cannot be taken into account in the stability formulation of section 3.1, since l is not explicitly known a priori. It is assumed that $l = 1$ in this formulation.

Considering the cutting force to be proportional to the chip thickness, the force components shown in figure 2 can be determined from

$$
\left\{
\begin{array}{c}
\Delta F_r^i(t, z; \tau_1, \tau_2) \\
\Delta F_t^i(t, z; \tau_1, \tau_2) \\
\Delta F_z^i(t, z; \tau_1, \tau_2)
\end{array}
\right\}
=
\begin{bmatrix}
1 & 0 & 0 \\
0 & \cos\eta & \sin\eta \\
0 & -\sin\eta & \cos\eta
\end{bmatrix}
\left\{
\begin{array}{c}
k_n \frac{\Delta z}{\cos\eta}(k_t h + C_p \dot{h}) \\
\frac{\Delta z}{\cos\eta}(k_t h + C_p \dot{h}) \\
\mu \frac{\Delta z}{\cos\eta}[\cos\varphi_n - k_n \sin\varphi_n](k_t h + C_p \dot{h})
\end{array}
\right\}
\tag{12}
$$

where k_t is the specific cutting energy, k_n is a proportionality factor, μ is the friction coefficient for sliding between the chip and the rake face of the cutting tooth, C_p is process damping coefficient, and φ_n is the normal rake angle of the cutting tooth [13]. Here, the forces along the axis of the cutting tool are not considered further because the focus is on the dynamics in the horizontal plane.

For each section of a flute shown in figure 2, the cutting force components ΔF_x^i and ΔF_y^i along the directions of the inertial frame can be determined through the transformation

$$
\left\{
\begin{array}{c}
\Delta F_x^i(t, z; \tau_1, \tau_2) \\
\Delta F_y^i(t, z; \tau_1, \tau_2)
\end{array}
\right\}
=
\begin{bmatrix}
-\sin\theta(t, i, z) & -\cos\theta(t, i, z) \\
-\cos\theta(t, i, z) & \sin\theta(t, i, z)
\end{bmatrix}
\left\{
\begin{array}{c}
\Delta F_r^i(t, z; \tau_1, \tau_2) \\
\Delta F_t^i(t, z; \tau_1, \tau_2)
\end{array}
\right\}
\tag{13}
$$

The cutting force components shown in equations (13) are spatially integrated along the axis of the tool to obtain the cutting force components F_x^i and F_y^i associated with each cutter flute i. The limits for spatial integration depend upon the workpiece–tool system dynamics as discussed by Balachandran and Zhao [13].

On substituting equations (3)–(6) in equations (1), the resulting system is

$$
\begin{aligned}
\mathbf{M}\ddot{\mathbf{q}}(t) &+ [\mathbf{C} - \hat{\mathbf{C}}(t)]\dot{\mathbf{q}}(t) + [\mathbf{K} - \hat{\mathbf{K}}(t)]\mathbf{q}(t) \\
&= \hat{\mathbf{C}}_1(t)\dot{\mathbf{q}}(t - \tau_1) + \hat{\mathbf{C}}_2(t)\dot{\mathbf{q}}(t - \tau_2) + \hat{\mathbf{K}}_1(t)\mathbf{q}(t - \tau_1) \\
&\quad + \hat{\mathbf{K}}_2(t)\mathbf{q}(t - \tau_2) + \mathbf{K}f\tau_1
\end{aligned}
\tag{14}
$$

where $\mathbf{q} = [q_x\ q_y\ q_u\ q_v]^T$, $\mathbf{M}$ is the diagonal inertia matrix, $\mathbf{K}$ is the stiffness matrix, and $\mathbf{C}$ is the damping matrix.

Introducing the state vector,

$$\mathbf{Q} = \left\{ \begin{array}{c} \mathbf{q} \\ \dot{\mathbf{q}} \end{array} \right\} \tag{15}$$

equations (14) can be rewritten as

$$\mathbf{Q}(t) = \mathbf{W}_0(t)\mathbf{Q}(t) + \mathbf{W}_1(t)\mathbf{Q}(t - \tau_1) + \mathbf{W}_2(t)\mathbf{Q}(t - \tau_2) + \left\{ \begin{array}{c} 0 \\ \bar{\kappa}(t) \end{array} \right\} f\tau_1 \tag{16}$$

where $\mathbf{W}_0(t)$ is the coefficient matrix for the vector of present states

$$\mathbf{W}_0(t) = \begin{bmatrix} 0 & \mathbf{I} \\ -\mathbf{M}^{-1}(\mathbf{K} - \hat{\kappa}(t)) & -\mathbf{M}^{-1}(\mathbf{C} - \hat{\mathbf{C}}(t)) \end{bmatrix} \tag{17}$$

and $\mathbf{W}_1(t)$ and $\mathbf{W}_2(t)$ are the coefficient matrices associated with vectors of delayed states. These matrices are given by

$$\mathbf{W}_1(t) = \begin{bmatrix} 0 & 0 \\ -\mathbf{M}^{-1}\hat{\kappa}_1(t)) & -\mathbf{M}^{-1}\hat{\mathbf{C}}_1(t)) \end{bmatrix} \tag{18}$$

$$\mathbf{W}_2(t) = \begin{bmatrix} 0 & 0 \\ -\mathbf{M}^{-1}\hat{\kappa}_2(t)) & -\mathbf{M}^{-1}\hat{\mathbf{C}}_2(t)) \end{bmatrix} \tag{19}$$

The matrices $\mathbf{W}_0(t)$, $\mathbf{W}_1(t)$, and $\mathbf{W}_2(t)$ contain T-periodic and piecewise linear functions.

2.2 Model with Variable Time Delay

In this case, the time delay is a function of the angular coordinate θ and it is given by

$$\tau = \frac{2\pi R}{N[2\pi R\Omega + f\cos\theta(t, i, z)]} \tag{20}$$

This delay is based on the observation that the angular speed on the periphery of the cutting tool is different at each angular position, as a result of the feed rate.

The governing equations of the system shown in figure 1 take the form

$$\begin{array}{ccccccc} m_x\ddot{q}_x & + & c_x\dot{q}_x & + & k_xq_x & = & F_x(t;\tau) \\ m_y\ddot{q}_y & + & c_y\dot{q}_y & + & k_yq_y & = & F_y(t;\tau) \\ m_u\ddot{q}_u & + & c_u\dot{q}_u & + & k_uq_u & = & F_u(t;\tau) \\ m_v\ddot{q}_v & + & c_v\dot{q}_v & + & k_vq_v & = & F_v(t;\tau) \end{array} \tag{21}$$

Equations (9), (10), and (3) get respectively modified to the following:

$$h(t, i, z; \tau) = A(t; \tau)\sin\theta(t, i, z) + B(t; \tau)\cos\theta(t, i, z) \tag{22}$$

$$\theta(t, i, z) = 2\pi\Omega t - (i - 1)\frac{2\pi}{N} - \frac{\tan\eta}{R}z + \theta_0 \tag{23}$$

$$A(t; \tau) = q_x(t) - q_x(t - l\tau) + q_u(t) - q_u(t - l\tau) + lf\tau$$
$$B(t; \tau) = q_y(t) - q_y(t - l\tau) + q_v(t) - q_v(t - l\tau) \tag{24}$$

Similarly, the other equations shown in section 2.1 can be modified appropriately after replacing the discrete delays τ_1 and τ_2 with the variable time delay given by equation (20).

3 STABILITY ANALYSIS

The system of equations (16) is a non-linear, non-homogeneous and non-autonomous delay-differential equations with time-periodic coefficients. For a chosen set of control parameters, which are typically the spindle speed and the axial depth of cut (ADOC), the stability of a periodic solution of this system of equations is to be determined. In section 3.1, the semi-discretization method presented by Insperger and Stépán [17, 18] is used to determine the local stability of a periodic motion. Here, this method is extended to handle systems with two discrete time delays, and further, this scheme is applied to a system with loss-of-contact non-linearities [20]. In section 3.2, the integral operator method is presented for determining the stability of a periodic solution of a delay-differential system with two discrete time delays. Stability of periodic solutions of the system (21) with a variable time delay is not addressed here, but it is to be treated in a future publication [21].

Let the nominal periodic solution of equations (16) be represented by $\mathbf{Q}_0(t)$. Then, a perturbation $\mathbf{X}(t)$ is provided to this nominal solution resulting in

$$\mathbf{Q}(t) = \mathbf{Q}_0(t) + \mathbf{X}(t) \tag{25}$$

After substituting equations (25) into (16), the resulting system governing the perturbation is given by

$$\dot{\mathbf{X}}(t) = \mathbf{W}_0(t)\mathbf{X}(t) + \mathbf{W}_1(t)\mathbf{X}(t - \tau_1) + \mathbf{W}_2(t)\mathbf{X}(t - \tau_2) \tag{26}$$

The extended Floquet theory presented by Hahn [15] and Farkas [22] provides a basis for determining the stability of the trivial solution $\mathbf{X}(t) = \mathbf{0}$ of the system (26). If all of the Floquet multipliers are within the unit circle, then the corresponding periodic solution of (16) is stable. If one or more of the Floquet multipliers are on the unit circle, while the rest of them are inside the unit circle, then the corresponding periodic solution may undergo a bifurcation [23].

Similar to the monodromy matrix [23] for finite-dimensional systems, an operator called the U operator can be defined for delay-differential systems (see section 3.2). The question is how to determine a finite-dimensional approximation for this operator, which has no closed-form solutions. In section 3.1, this finite-dimensional approximation is sought by using the semi-discretization method. The eigenvalues (characteristic multipliers) of this matrix can be used to examine the local stability of the considered periodic solution. In section 3.2, approximations for these eigenvalues are determined by using the integral operator method.

3.1   Semi-Discretization Formulation

In this formulation, the time period T of the periodic orbit is first broken up into $(k + 1)$ intervals each of length Δt, and in each interval, the non-autonomous delay-differential system (26) is replaced by an autonomous ordinary differential system. This piecewise linear system of ordinary differential equations is solved to obtained a high-dimensional linear map, which is examined for determining stability of $\mathbf{X}(t) = 0$ of the system (26).

As illustrated in figure 3, the time interval Δt is chosen as

$$\Delta t = \frac{\tau_1}{N1 + \frac{1}{2}} \tag{27}$$

where $N1$ is the number of steps selected to approximate the delay τ_1. The relationship between Δt and the other discrete time delay τ_2 is given by

$$\tau_2 = \left(N2 + \frac{1}{2} + yr \right) \times \Delta t \tag{28}$$

where yr is given by

$$yr = \mathrm{mod} \left(\frac{\tau_2 - 1/2\Delta t}{\Delta t} \right) \tag{29}$$
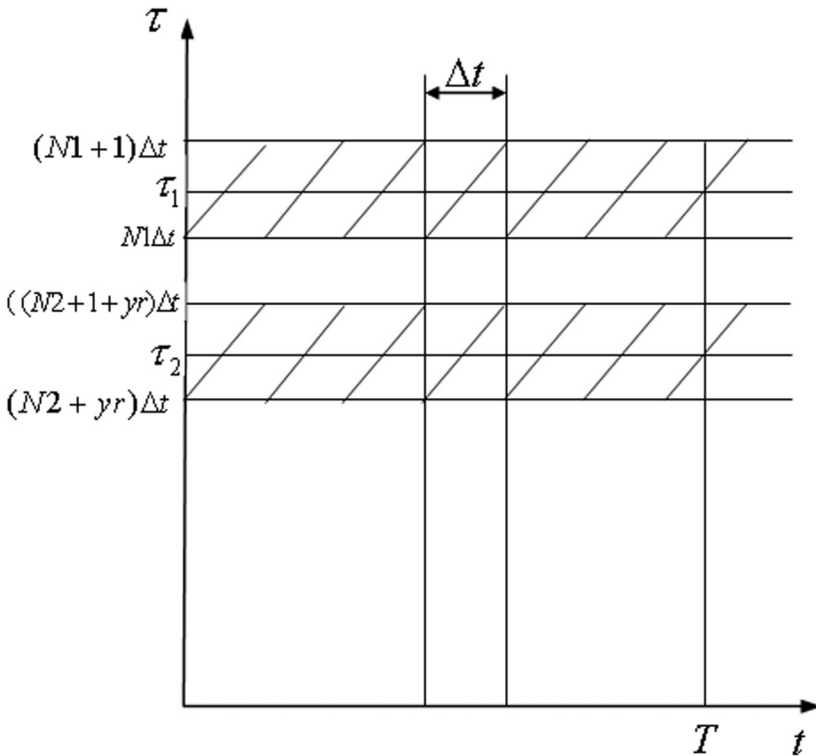
Figure 3. Discretization scheme.

and

$$N2 = \frac{\tau_2}{\Delta t} - yr - \frac{1}{2} \tag{30}$$

For $t \in [t_i, t_{i+1}]$, the delayed states are approximated as

$$x(t - \tau_1) \simeq x(t_i + 1/2\Delta t - \tau_1) = x(t_{i-N1}) \tag{31}$$

$$x(t - \tau_2) \simeq x(t_i + 1/2\Delta t - \tau_2) = x(t_{i-N2} - yr) \tag{32}$$

$$\simeq (1 - yr)x(t_{i-N2}) + yr \cdot x(t_{i-N3}) \tag{33}$$

and $N3 = N2 + 1$.

The time-periodic terms in equations (26) are approximated as

$$\mathbf{W}_{i,0} = \mathbf{W}_0(t_i) \simeq \frac{1}{\Delta t} \int_{t_i}^{t_{i+1}} \mathbf{W}_0(t)dt \tag{34}$$

$$\mathbf{W}_{i,N1} = \mathbf{W}_{N1}(t_i) \simeq \frac{1}{\Delta t} \int_{t_i}^{t_{i+1}} \mathbf{W}_1(t)dt \tag{35}$$

$$\mathbf{W}_{i,N2} = \mathbf{W}_{N2}(t_i) \simeq \frac{(1 - yr)}{\Delta t} \int_{t_i}^{t_{i+1}} \mathbf{W}_2(t)dt \tag{36}$$

$$\mathbf{W}_{i,N3} = \mathbf{W}_{N3}(t_i) \simeq \frac{yr}{\Delta t} \int_{t_i}^{t_{i+1}} \mathbf{W}_2(t)dt \tag{37}$$

Then, over each time interval $t \in [t_i, t_{i+1}]$ for $i = 0,1,2,\ldots,k$, equations (26) can be approximated as

$$\mathbf{X}(t) = \mathbf{W}_{i,0}\mathbf{X}(t) + \mathbf{W}_{i,N1}\mathbf{X}_{i-N1} + \mathbf{W}_{i,N2}\mathbf{X}_{i-N2} + \mathbf{W}_{i,N3}\mathbf{X}_{i-N3} \tag{38}$$

where $\mathbf{X}(t_i)$ is represented by $\mathbf{X}_i$. Thus, the infinite-dimensional system (26) has been replaced by a piecewise system of ordinary differential equations in the time period $t \in [t_0, t_0 + T]$. Note that in each interval, the autonomous system has a constant excitation or forcing term that arises due to the delay effects.

To proceed further, it is assumed that $\mathbf{W}_{i,0}$ is invertible for all i. Then, the solution of equations (38) takes the form

$$\mathbf{X}(t) = e^{\mathbf{W}_{i,0}(t-t_i)}[\mathbf{X}_i + \mathbf{W}_{i,0}^{-1} \sum_{j=1}^{N1} \mathbf{W}_{i,j}\mathbf{X}_{i-j}] - \mathbf{W}_{i,0}^{-1} \sum_{j=1}^{N1} \mathbf{W}_{i,j}\mathbf{X}_{i-j} \tag{39}$$

When $t = t_{i+1}$, the system (39) leads to

$$\mathbf{X}_{i+1} = \mathbf{M}_{i,0}\mathbf{X}_i + \sum_{j=1}^{N1} \mathbf{M}_{i,j}\mathbf{X}_{i-j} \tag{40}$$

where the associated matrices are given by

$$\mathbf{M}_{i,0} = \exp(\mathbf{W}_{i,0}\Delta t) \tag{41}$$

and for $j > 0$,

$$\mathbf{M}_{i,j} = \begin{cases} \exp(\mathbf{W}_{i,0}\Delta t - I)\mathbf{W}_{i,0}^{-1}\mathbf{W}_{i,j} & \text{if } j = N1, N2, N3 \\ 0 & \text{otherwise} \end{cases} \tag{42}$$

The system (40) can be used to construct the state vector

$$\mathbf{Y}_i = (\mathbf{X}_i^T, \mathbf{X}_{i-1}^T, \dots, \mathbf{X}_{i-N1}^T)^T \tag{43}$$

and the linear map

$$\mathbf{Y}_{i+1} = \mathbf{B}_i\mathbf{Y}_i \tag{44}$$

where the $\mathbf{B}_i$ matrix is given by

$$\mathbf{B}_i = \begin{bmatrix} \mathbf{M}_{i,0} & 0 & \cdots & \mathbf{M}_{i,N2} & \mathbf{M}_{i,N3} & \cdots & 0 & \mathbf{M}_{i,N1} \\ \mathbf{I} & 0 & \cdots & 0 & 0 & \cdots & 0 & 0 \\ 0 & \mathbf{I} & \cdots & 0 & 0 & \cdots & 0 & 0 \\ \vdots & \vdots & \ddots & \vdots & \vdots & \ddots & \vdots & \vdots \\ 0 & 0 & \cdots & \mathbf{I} & 0 & \cdots & 0 & 0 \\ 0 & 0 & \cdots & 0 & \mathbf{I} & \cdots & 0 & 0 \\ \vdots & \vdots & \ddots & \vdots & \vdots & \ddots & \vdots & \vdots \\ 0 & 0 & \cdots & 0 & 0 & \cdots & \mathbf{I} & 0 \end{bmatrix} \tag{45}$$

For a 'small' feed rate, $\tau_1 \leq \tau_2 + \delta t$, and hence, $N1 = N3$. In this case, the matrix $\mathbf{B}_i$ can be shown to be

$$\mathbf{B}_i = \begin{bmatrix} \mathbf{M}_{i,0} & 0 & \cdots & \mathbf{M}_{i,N2} & \mathbf{M}_{i,N3} + \mathbf{M}_{i,N1} \\ \mathbf{I} & 0 & \cdots & 0 & 0 \\ 0 & \mathbf{I} & \cdots & 0 & 0 \\ \vdots & \vdots & \ddots & \vdots & \vdots \\ 0 & 0 & \cdots & \mathbf{I} & 0 \end{bmatrix} \tag{46}$$

From the system (44), it follows that

$$\mathbf{Y}_{k+1} = \mathbf{B}_k \cdots \mathbf{B}_1\mathbf{B}_0\mathbf{Y}_0 \tag{47}$$

from which the transition matrix can be identified as

$$\Phi = \mathbf{B}_k \cdots \mathbf{B}_1\mathbf{B}_0 \tag{48}$$

This matrix Φ represents a finite-dimensional approximation of the 'monodromy matrix' associated with the periodic orbit $\mathbf{Q}_0(t)$ of (16) and the trivial solution $\mathbf{X}(t) = 0$ of (26). If the eigenvalues of this matrix are all within the unit circle, then the trivial fixed point of (26) is stable, and hence, the associated periodic orbit of (16) is stable. At

a bifurcation point, one or more of the eigenvalues of the transition matrix will be on the unit circle. Here, the hypothesis is that post-bifurcation motions are associated with chatter.

3.2 Integral Operator Formulation

In the system (26), let $W_0(t)$, $W_1(t)$ and $W_2(t)$ be periodic with period T and suppose

$$\tau_2 < \tau_1 \leq T \tag{49}$$

The variation of constants formula for (26) with an initial value at t = 0 (see Halanay [24]) is

$$
\begin{aligned}
X(t) = \Psi(t,0)X(0) &+ \int_{-\tau_1}^{0} \Psi(t, s+\tau_1)W_1(s+\tau_1)X(s)ds \\
&+ \int_{-\tau_2}^{0} \Psi(t, s+\tau_2)W_2(s+\tau_2)X(s)ds
\end{aligned}
\tag{50}
$$

The variation of constants formula (50) can also be written as

$$
\begin{aligned}
X(t) = \Psi(t,0)X(0) &+ \int_{-\tau_1}^{-\tau_2} \Psi(t, s+\tau_1)W_1(s+\tau_1)X(s)ds \\
&+ \int_{-\tau_2}^{0} [\Psi(t, s+\tau_1)W_1(s+\tau_1) + \Psi(t, s+\tau_2)W_2(s+\tau_2)]X(s)ds
\end{aligned}
\tag{51}
$$

The function $\Psi(t, 0)$ is the matrix solution of (26) such that $\Psi(0, 0) = I$, $\Psi(t, 0) = 0$ for $t < 0$, where I is the identity matrix. This matrix function must be computed numerically for any significant delay equation of the form (26). The function dde23 (see Shampine and Thompson [25]) stores intermediate values that allow interpolations by, for example, splines of other intermediate values as needed.

Let $\phi(t)$ be an initial history function in the space of continuous functions on $[-\tau_1, 0]$. Define the operator

$$(U\phi)(s) = X(s+T; \phi) \tag{52}$$

where the notation $X(t; \phi)$ indicates the solution of (26) with the initial history function ϕ on the interval $[-\tau_1, 0]$. Then, using (51) one can write

$$
\begin{aligned}
(U\phi)&(s) \\
&= \Psi(s+T,0)\phi(0) + \int_{-\tau_1}^{-\tau_2} \Psi(s+T, s+\tau_1)W_1(s+\tau_1)\phi(s)ds \\
&+ \int_{-\tau_2}^{0} [\Psi(s+T, s+\tau_1)W_1(s+\tau_1) + \Psi(s+T, s+\tau_2)W_2(s+\tau_2)]\phi(s)ds
\end{aligned}
\tag{53}
$$

If there is a non-trivial solution $X(t; \phi)$ of (26) such that $X(t+T; \phi) = \rho X(t; \phi)$ for all t then ρ is a characteristic multiplier of (26). Halanay [24] has shown that it is

sufficient to take $t \in [-\tau_1, 0]$. The characteristic multipliers of (26) are then the eigenvalues of the operator U defined in (52).

As is often done to find the eigenvalues of an integral operator, the method of quadratures will be used to approximate the eigenvalues of (53) by discretizing $[-\tau_1, 0]$ with an an even mesh

$$-\tau_1 = s_1 < s_2 < \cdots < s_{NN+1} = 0, \tag{54}$$

where $s_{i+1} - s_i = \Delta = \tau_1 / NN$ for $i = 1, 2, \ldots, NN$. The operator U in (53) can be represented by a matrix equation

$$\begin{pmatrix} (U\phi)(s_1) \\ \vdots \\ (U\phi)(s_i) \\ \vdots \\ (U\phi)(s_{NN+1}) \end{pmatrix} = \begin{bmatrix} U_{1,1} & \cdots & U_{1,j} & \cdots & U_{1,NN+1} \\ \vdots & \cdots & \vdots & \cdots & \vdots \\ U_{i,1} & \cdots & U_{i,j} & \cdots & U_{i,NN+1} \\ \vdots & \cdots & \vdots & \cdots & \vdots \\ U_{NN+1,1} & \cdots & U_{NN+1,j} & \cdots & U_{NN+1,NN+1} \end{bmatrix} \begin{pmatrix} \phi(s_1) \\ \cdots \\ \phi(s_i) \\ \cdots \\ \phi(s_{NN+1}) \end{pmatrix}. \tag{55}$$

Each $U_{i,j}$ is a block matrix in itself and they are defined as follows. Let k be such that

$$s_{k-1} < -\tau_2 \leq s_k \tag{56}$$

The ith block row of the matrix equation is given by the discretized form of (51) as

$$\begin{aligned} (U\phi)(s_i) = & \Delta \sum_{j=1}^{k-1} \Psi(s_i + T, s_j + \tau_1) W_1(s_j + \tau_1) \phi(s_j) \\ & + \Delta \sum_{j=k}^{NN} \left[\Psi(s_i + T, s_j + \tau_1) W_1(s_j + \tau_1) \right. \\ & \left. + \Psi(s_i + T, s_j + \tau_2) W_2(s_j + \tau_2) \right] \phi(s_j) \\ & + \left[\Psi(s_i + T, 0) + \Psi(s_i + T, s_{NN+1} + \tau_1) W_1(s_{NN+1} + \tau_1) \right. \\ & \left. + \Psi(s_i + T, s_{NN+1} + \tau_2) W_2(s_{NN+1} + \tau_2) \right] \phi(s_{NN+1}). \end{aligned} \tag{57}$$

The $U_{i,j}$ blocks are defined as follows:

$$U_{i,j} = \begin{cases} \Psi(s_i + T, s_j + \tau_1) W_1(s_j + \tau_1) & j = 1, \cdots, k-1 \\ \begin{aligned} & \Psi(s_i + T, s_j + \tau_1) W_1(s_j + \tau_1) \\ & + \Psi(s_i + T, s_j + \tau_2) W_2(s_j + \tau_2) \end{aligned} & j = k, \cdots, NN \\ \begin{aligned} & \Psi(s_i + T, 0) + \Psi(s_i + T, s_{NN+1} + \tau_1) W_1(s_{NN+1} + \tau_1) \\ & + \Psi(s_i + T, s_{NN+1} + \tau_2) W_2(s_{NN+1} + \tau_2) \end{aligned} & j = NN + 1 \end{cases} \tag{58}$$

We note that, since $0 < s_i + T \leq T$ and $s_{NN+1} = 0$, all values of the Ψ function in the block rows above the $i = NN + 1$ row can be obtained by interpolation from stored numerical integration values. That is the significance of using a function like dde23 that stores intermediate values. This reduces the computation involved since the integration of (26) is the most time consuming operation. The time savings becomes noticeable for large values of NN. Once the matrix of $U_{i,j}$ blocks is set up, the eigenvalues of the matrix approximate the characteristic multipliers of (26). As

discussed in section 3.1, these eigenvalues can then be used to determine the stability of the periodic solution of (16).

4 Representative results

In this section, representative results obtained through numerical investigations into the dynamics and stability of various milling operations are presented. The tool–workpiece system modal parameters are shown in table 1, and the tool and cutting parameters are shown in table 2. The feed rate is fixed at 0.102 mm/tooth for all of the different cases. The stability charts are presented in the space of axial depth of cut (ADOC) and the spindle speed. These charts were constructed by using two approaches, one through direct numerical integration of (14) and another through the semi-discretization analysis of section (3.1). Each point on the chart corresponds to the location where the periodic motion of (14) loses stability, when the ADOC is varied while holding the spindle speed constant. Above a stability lobe, the periodic motion of the system is unstable, and below a stability lobe, the periodic motion of the system is stable.

In figures 4 and 5, stability charts are presented for 25% immersion operations. These results correspond to up-milling and down-milling milling operations (i.e. opposite directions of spindle rotation). As first reported by Zhao and Balachandran [14], stability charts generated for up-milling operations and down-milling operations can be different and this is confirmed by the results presented in figures 4 and 5. In addition, the occurrence of period-doubling bifurcations is indicated by time-domain simulations and confirmed by the results of the semi-discretization analysis. The period-doubling bifurcation points are marked by stars in the figures. At the other locations on the stability lobes, secondary Hopf bifurcations occur. A more complete discussion of results such as those shown here can be found in the work of Long and Balachandran [20].

Table 1: Modal parameters of workpiece–tool system.

Mode	Frequency (Hz)	Damping (%)	Stiffness (N/m)	Mass (kg)
tool (X)	1006.58	1.0	8.0×10^5	2.0×10^{-2}
tool (Y)	1027.34	1.5	1.0×10^6	2.4×10^{-2}
workpiece (U)	503.29	1.0	1.0×10^6	1.0×10^{-1}
workpiece (V)	711.76	1.0	3.0×10^6	1.5×10^{-1}

Table 2: Tool and cutting parameters.

Normal rake angle (φn)	Helix angle (η)	Tool number	Radius (mm)	Kt (Mpa)	kn	Cutting friction coefficient (μ)
15°	30°	2	6.35	600	0.3	0.2
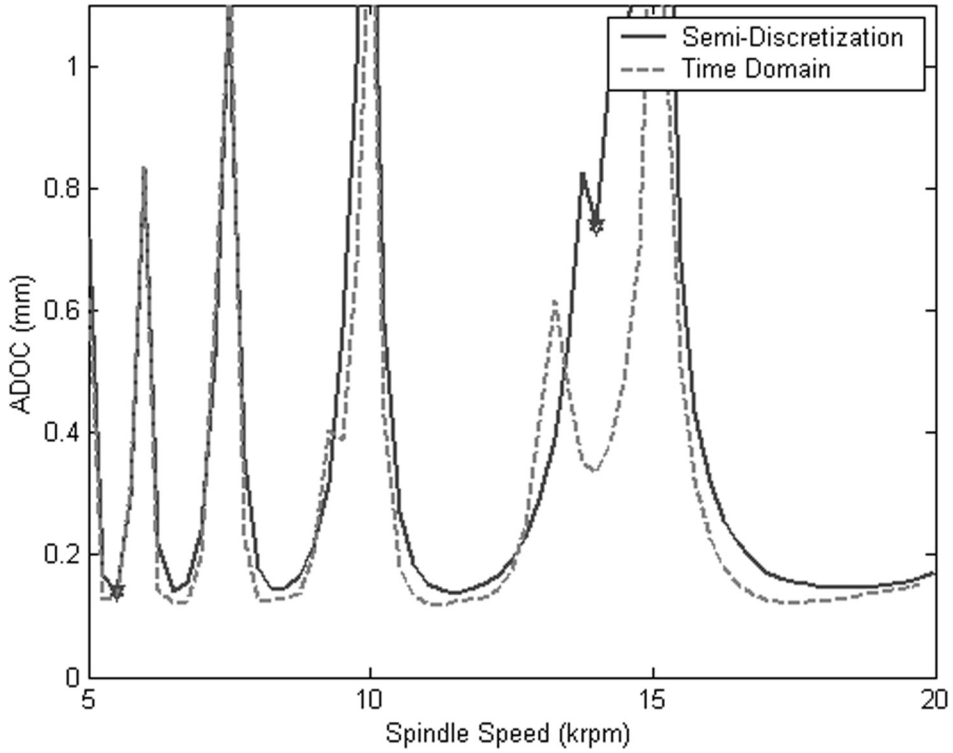
Figure 4. Stability charts for 25% immersion up-milling operations.
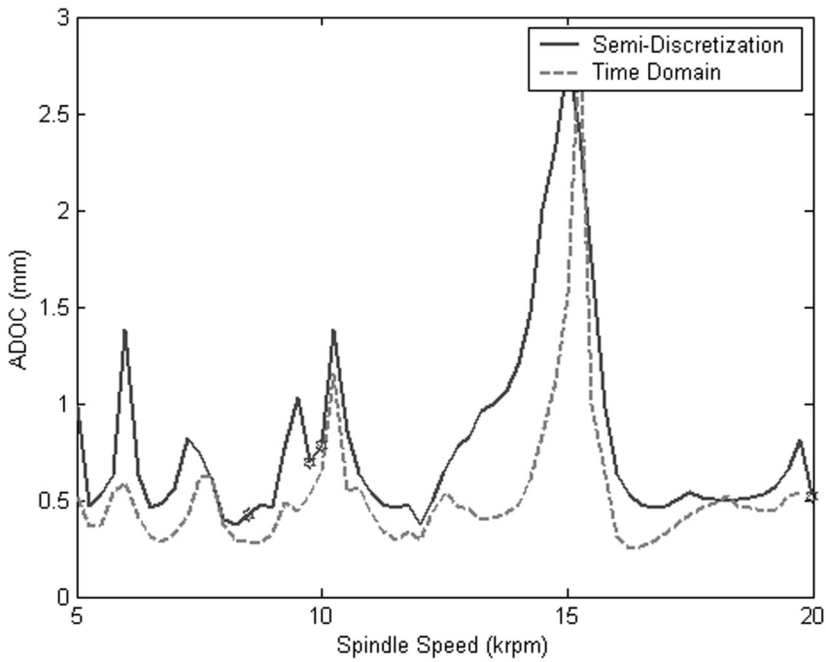
Figure 5. Stability charts for 25% immersion down-milling operations.

5   Closure

Two mathematical models that can be used to study non-linear oscillations of milling have been presented and discussed in this work. Sources of non-linearities and dependence of the time-delay effect on the feed rate have also been explained here. The variable time-delay model is a new model that has been introduced here. Stability formulations that can be used to assess the stability of periodic orbits of delay differential systems with multiple delays have also been detailed. The models and the stability formulations are believed to be important for understanding instabilities leading to chatter in milling operations. In addition, consideration of feed rate effects in the model may help explore feed-rate controlled dynamics in high-speed milling.

Acknowledgements

References

[1] Kahles, J. F., Field, M. and Harvey, S. M., 1978, High speed machining possibilities and needs. *Annals of the CIRP*, **27**, 551 – 558.

[2] King, R. I., 1985, *Handbook of High-Speed Machining Technology* (New York: Chapman and Hall).

[3] Schulz, H., 1993. High-speed machining. *Annals of the CIRP*, **42**, 637 – 645.

[4] Komanduri, R., McGee, J., Thompson, R. A., Covy, J. P., Truncale, F. J., Tipnis, V. A., Stach, R. M. and King, R. I., 1985, On a methodology for establishing the machine tool system requirements for high-speed/high-throughput machining. *ASME Journal of Engineering for Industry*, **107**, 316 – 324.

[5] Tlusty, J. and Polacek, M., 1963, The stability of the machine tool against self-excited vibration in machining. *Proceedings of the Conference on International Research in Production Engineering, Pittsburgh, PA*, pp. 465 – 474 (ASME).

[6] Tobias, S. A., 1965, *Machine-Tool Vibration* (New York: Wiley).

[7] Opitz, H., Dregger, E.U. and Roese, H., 1966, Improvement of the dynamic stability of the milling process by irregular tooth pitch. *Proceedings of the 7th International MTDR Conference* (New York: Pergamon Press).

[8] Sridhar, R., Hohn, R. E. and Long, G. W., 1968, A stability algorithm for the general milling process. *ASME Journal of Engineering for Industry*, **90**, 330 – 334.

[9] Hanna, N. H. and Tobias, S. A., 1974, A theory of nonlinear regenerative chatter. *ASME Journal of Engineering for Industry*, **96**, 247 – 255.

[10] Minis, I. and Yanushevsky, R., 1993, A new theoretical approach for the prediction of machine tool chatter in milling. *ASME Journal of Engineering for Industry*, **115**, 1 – 8.

[11] Altintas, Y. and Budak, E., 1995, Analytical prediction of stability lobes in milling. *Annals of CIRP*, **44**, 357 – 362.

[12] Balachandran, B., 2001, Nonlinear dynamics of milling processes. *Philosophical Transactions of the Royal Society, London, A*, **359**, 793 – 819.

[13] Balachandran, B. and Zhao, M. X., 2000, A mechanics based model for study of dynamics of milling operations. *Meccanica*, **35**, 89 – 109.

[14] Zhao, M. X. and Balachandran, B., 2001, Dynamics and stability of milling process. *International Journal of Solids and Structures*, **38**, 2233 – 2248.

[15] Hahn, W., 1961, On difference-differential equations with periodic coefficients. *Journal of Mathematical Analysis and Applications*, **3**, 70 – 101.

[16] Nayfeh, A. H. and Mook, D. T., 1979, *Nonlinear Oscillations* (New York: Wiley).

[17] Insperger, T. and Stépán, G., 2002, Semi-discretization method for delayed systems. *International Journal of Numerical Methods in Engineering*, **55**, 503 – 518.

[18] Insperger, T. and Stépán, G., 2003, Stability of the damped Mathieu equation with time delay. *ASME Journal of Dynamic Systems, Measurement, and Control*, **166**, 166 – 171.

[19] Gilsinn, D., 2004, Approximating limit cycles of a van der Pol equation with delay. *Proceedings of Dynamic Systems and Applications 4* (Altanta).

[20] Long, X.-H. and Balachandran, B., Stability analysis of milling process. *Nonlinear Dynamics*, accepted for publication, 2002.

[21] Long, X. -H. and Balachandran, B., Milling dynamics with a variable time delay. Proceedings of ASME IMECE 2004, Anaheim, CA, November 13 – 19, Paper No. IMECE 2004-59207.

[22] Farkas, M.: *Periodic Motions* Springer-Verlag, New York, 1994.

[23] Nayfeh, A. H. and Balachandran, B., 1995, *Applied Nonlinear Dynamics: Analytical, Computational, and Experimental Methods* (New York: Wiley).

[24] Halanay, S., 1966, *Differential Equations, Oscillations, Time Lags* (New York, Academic Press).

[25] Shampine, L. F. and Thompson, S., 2001, Solving DDE's in MATLAB. *Applied Numerical Mathematics*, **37**, 441 – 458.